RSC Advances

RSC Advances

RSC**Publishing**

ARTICLE

Micro-Mesoporous Carbons for Controlled Release of Antipyrine and Indomethacin

Dipendu Saha[a]*, Tara Moken[a], Jihua Chen[b], Dale K. Hensley[b], Kristen Delaney[c], Marcus A. Hunt[c], Karl Nelson[a], Amada Spurri[a], Lauren Benham[a], Robin Brice[c], Martina Azoro[c]

We have demonstrated the potential of meso- and microporous carbons in controlled release applications and targeted for oral drug delivery. We have employed two mesoporous and two microporous carbons for sustained release of one aqueous soluble drug (antipyrine) and one aqueous insoluble drug (indomethacin) as models to examine the controlled release characteristics. The micro-mesoporous carbons were characterized with BET surface area of 372-2251 m^2/g and pore volume 0.63-1.03 cm^3/g. The toxicity studies with *E. Coli* bacterial cells did not reveal significant toxicity that is in accordance with our previous studies human cells with similar materials. Mucin adsorption tests with type III pork mucin demonstrated 20-30% mucin adsorption by the carbon samples and higher mucin adsorption could be attributed to higher surface area and oxygen functionalities. Antipyrine and indomethacin loading was 6-78% in these micro-mesoporous carbons. The signatures in thermogravimetric studies revealed the presence of drug molecules within the porous moieties of carbon. The partial shifting of decomposition peak of drug adsorbed within the carbon pores was caused by the confinement of drug molecules within the narrow pore space of carbons. The release profiles of both drugs were examined in simulated gastric fluid (pH=1.2) and in three other release media with the respective pH values of 4.5, 6.8 and 7.4 along with varying residence time to simulate the physiological conditions stomach, duodenum, small intestine and colon, respectively. All the release profiles manifested diffusion controlled sustained release that corroborates the effective role of micro-mesoporous carbons as potential drug carriers.

1. Introduction

Controlled and sustained release of bioactive agents, including drug, enzyme and related materials is one of the major challenges of human health care and medical sciences. An active and direct drug administration may provide a very high (toxic) or very low (ineffective) drug concentration in physiological system[1]. Repeated dose of active drug may result its concentration profile a saw-tooth type that is also not effective[1]. Nanoporous materials have widely been employed in the controlled release of several drug and related materials. The drug delivery from nanoporous materials is controlled by the adsorption and desorption mechanism within the nanosized pores of the material. During 'loading' or adsorption of the drug, it is stored within the nanopores in molecular form whereas its release within the physiological media is controlled by the diffusion and thermodynamics of the system[2]. For aqueous soluble drugs, diffusion barrier helps to maintain the sustained release. In the case of aqueous insoluble drugs, the molecular storing mechanism helps to overcome the high crystallization energy and enhance their release rates. The other benefits associated with the nanoporous media driven drug delivery system could be counted towards its ability to float in the gastrointestinal (GI) system owing its lower bulk density[2,3] and protecting the biological payload from different types of physiological degradation agents, like enzymes or immune systems[2].

The largest number of reports that incorporated porous materials as drug delivery agents are different kinds of mesoporous silica for multitude of drugs[4,5,6,7,8,9]. However, owing to the associated

[a] Department of Chemical Engineering, Widener University, PA 19013, USA. *E-mail: dsaha@mail.widener.edu, Tel: +1 610 499 4056, Fax: +1 610 499 4059
[b] Center for Nanophase Materials Sciences, Oak Ridge National Laboratory Oak Ridge, TN 37831, USA.
[c] Department of Biological Sciences, Fayetteville State University, 1200 Murchison Road Fayetteville, NC 28301, USA

drawbacks of silica-based systems, recently, nanoporous or mesoporous carbons have been reported to successfully act as passive drug delivery vehicles. Aimed towards oral drug delivery, ibuprofen[10,11], Indomethacin[11] and lovastatin[12] were successfully delivered from mesoporous carbons. Few anticancer drugs, like, doxorubicin[13], campthothecin[14] and mitoxantrone[15] were also successfully delivered from nanoporous carbons targeted towards blood plasma or transmembrane delivery. Our past research demonstrated that soft-templated mesoporous carbons can successfully maintain controlled release of four different drugs, captopril[16,17], furosemide[17], ranitidine hydrochloride[18] and antipyrine[18], aimed towards oral drug delivery. As biocompatibility of drug carrier is the fundamental prerequisite for its application, recently, we have demonstrated that mesoporous carbons are biocompatible and its biocompatibility is confirmed with the help of cytotoxicity study by HeLa cells, cell viability by fibroblast cells and hemocompatibility by hemolysis and blood protein adsorption studies[19].

   As a continued effort towards successfully establishing the nanoporous carbons as passive and controlled drug delivery media, we have employed two different drugs based on aqueous solubility, indomethacin (aqueous insoluble) and antipyrine (aqueous soluble). Figure 1(a) and (b) show the molecular configuration and geometric properties of these two drugs calculated by Spartan software. In order to investigate drug loading and release profiles, we have selected four different nanoporous carbons, two microporous and two other mesoporous carbons with varying specific surface area and pore widths. In order to target oral delivery, we have sequentially exposed the drug loaded nanoporous carbons in pH 1.2, 4.5, 6.8 and 7.4 in pre-determined time intervals to mimic the physiological conditions of stomach, duodenum, small intestine and colon, respectively[20].

Area: 353.77 Å^2
Volume: 339.30 Å^3
Ovality: 1.5
(a)

Area: 219.24 Å^2
Volume: 202.64 Å^3
Ovality: 1.31
(b)
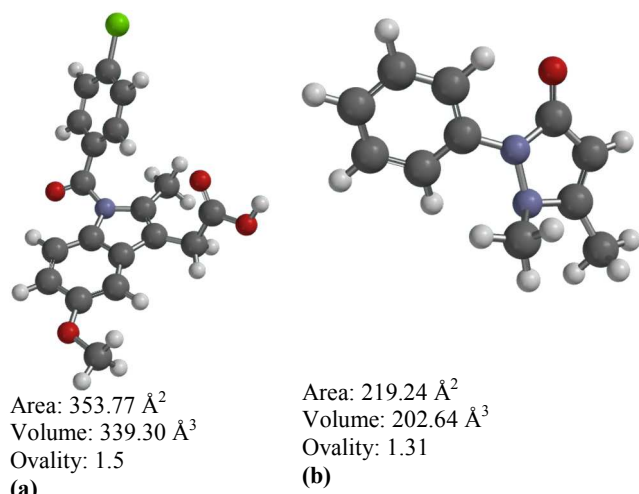
Figure 1: Molecular formula and geometric properties of indomethacin (a) and antipyrine (b) molecule. Color configuration: black-carbon; grey-hydrogen, red-oxygen, blue-nitrogen, green-chlorine. The molecular configuration and geometric properties are calculated in Spartan software.

2. Experimental

2.1 Synthesis of micro-meosporous carbons

         In order to synthesize the mesoporous carbons, we have employed previously employed strategy for phloroglucinol-F127 derived carbons[17,18]. Typically, 5.0 g phloroglucinol and 4.0 g Pluronic F127 were dissolved in 17 mL water/24 mL ethanol mixture with 0.5 mL 36% HCl as catalyst and stirred for 30 minutes. After that, 4.8 mL 37% formaldehyde added as cross-linking agent and continued stirring for 1 hour. The reaction mixture becomes turbid and the polymer layer is separated from solvents by simple sedimentation and aged for few days at room temperature. It is then put in a porcelain boat and carbonized in a tube furnace in N_2 atmosphere with the following temperature profile: room temperature to 400°C at 1°/min, 400°C to 1000°C at 2°C/min and keeping in final temperature for 5 minutes followed by cooling down to room temperature in the N_2 flow. This material is named as meso-C1. To activate this mesoporous carbon, it is ground and mixed with solid KOH in 1:3 ratio and heated in N_2 upto 1000 °C at a ramp rate of 10°C/min and cooling down to ambient temperature in N_2 flow. The activated mesoporous carbon is termed as meso-C2. In order to synthesize microporous carbons, we have employed polymerized furfuryl alcohol as carbon precursor. Typically, 20 mL furfuryl alcohol is ice cooled and 10 mL 0.19 g *p*-toluidine sulfonic acid in 10 mL tetrahydrofuran is added onto it dropwise over the time of 30 minutes as polymerization inducing agent. The stirring is continued overnight to enhance the degree of polymerization till it reaches a dark green to black colored viscous material. It is carbonized in the tube furnace in the same N_2 flow upto 1000 °C at 10°C/min and cooled in the same N_2 atmosphere. It is then mixed with solid KOH in 1:3 ratio and heated in the same fashion that of meso-C2. The resultant carbon is termed as micro-C1. In order to obtain another high surface area carbon, we have obtained a commercial chemically activated porous carbon from ACS Material®. It is washed with DI water several times and termed as micro-C2.

2.2 Characterization of micro-meosporous carbons

   The porosity of the nanoporous materials are obtained by N_2 adsorption-desorption at 77 K and CO_2 adsorption-desorption at 273 K in Quantachrome Autosorb iQ porosity and surface area analyzer. Porosity data including Brunauer-Emmett-Teller (BET) specific surface area and pore size distribution by non-local density functional theory (NLDFT) are calculated within the software of instrument. The transmission electron microscopic (TEM) images were captured in Carl Zeiss Libra 120 TEM microscope operating at 120 kV. The samples were dispersed in ethanol by ultrasonicating at 0.5 wt.% concentration and drop-casted on the amorphous carbon coated TEM grid (Ted Pella). The scanning electron microscopic (SEM) images are obtained in Carl Zeiss Merlin SEM operating at 30 kV. No additional sample preparation were employed for SEM, as-received samples were directly put on the SEM stand.

2.2 Cytotoxicity and mucoadhesive properties

   For this particular study, cytotoxicity studies were performed on *E. Coli* cells with a standard protocol. Typically, the porous carbon samples were ground in a mortar and pestle and 10 mg of carbon powder were added to 0.5 mL ethanol (95%) and sonicated for 10 minutes. The dispersion was added to the *E. Coli* suspension with carbon concentration of 50, 300 and 500 μg/mL along with a control sample without any carbon material. All the carbon-seeded and control bacterial samples were incubated for 24 hours and then bacterial concentrations were monitored by standard dilution and plating method and measured in triplicate. In order to facilitate imaging, trypan blue stain was added to the cells and the images were captured in an olympus bx-40 microscope with 1,000x magnification in transmitted light mode.

   Surface adsorption of mucin is an indirect measure of mucoadhesive properties of the drug carrier media[21, 22]. In a typical

experiment, 20 mg of pure carbons samples were stirred in a 20 cm³ 500 ppm mucin (Sigma-Aldrich, extracted from pork stomach, type III) solution in DI water for 12 hours at 37 °C. After that, the carbon particles are separated by filtration and the concentration of the mucin in the residual solution is measured to calculate the mucin adsorption by the carbons. All the mucin concentrations are measured by standard Bradford protein assay at 595 nm wavelength in a Thermo-scientific GENESYS 10S UV-Vis spectrophotometer. The mucin adsorption amount is calculated as: Adsorption % = [(Initial mucin – Final mucin)/Initial mucin]X100%

2.2 Drug loading and delivery

For indomethacin, nanoporous carbons (except for micro-C2) and pure drug were stirred at 6.5:1 ratio in 120 mL ethanol overnight and the carbons were separated from solvent by simple filtration. Because of high surface area and high loading of Micro-C2, the ratio was set to 1:1. Antipyrine was loaded by stirring carbon and pure drug in 3:1 ratio in DI water overnight and separated in the similar fashion. In order to measure the drug loading amount, 2 μL of elutant drug solution is mixed with either 20 mL ethanol (for indomethacin) or DI water (for antipyrine) and measured in Thermoscientific GENESYS 10S UV-Vis spectrophotometer against a pre-calibrated chart. The separated carbon materials are quickly washed with respective solvents to remove accumulated drug from the surface.

In order to visualize the presence of adsorbed drug molecules within the porous carbon moieties, thermograms of drug decomposition at high temperature are measured in the TA instruments' SDT Q600 instrument in N_2 flow. The thermograms of derivative wt.% of drug loaded carbons are compared with pure drug.

The media for the release experiments were composed of pH=1.2, 4.5, 6.8 and 7.4 for 3, 1, 3 and 5 hrs, respectively, representing physiological conditions of stomach, duodenum, small intestine and colon[20]. For all release experiments, the temperature of release medium was set to 37 °C to simulated body temperature. The medium with pH 1.2 (simulated gastric fluid, SGF) was formulated by mixing DI water with 1% NaCl and pH adjusted by HCl (without pepsin). The pH of the rest of the media was adjusted by HCl only without any enzyme. To perform the release experiments, drug loaded carbons were brought in contact with respective physiological media in 0.2 g dose/50 mL media (for indomethacin) or 0.1 g dose/50 mL media (for antipyrine). The stirring speed for pH=1.2 medium was 150 rpm whereas it was to 50 rpm for rest of the media[20]. For all the samples 3 cm³ of sample was taken out and immediately replenished with similar media. For micro-C2, an additional filtration was employed to separate the fine carbon particles before analysis. For indomethacin release experiments only, 3 cm³ of release medium is mixed 1 cm³ of ethanol (200 proof) before measuring the concentration in the UV-Vis spectroscope. All the concentration in the UV-Vis measurement was calculated based on a pre-calibrated chart, prepared for each kind of release media. Owing to the high concentration of released antipyrine in Micro-C2/antipyrine release experiments, 100 μL of release medium is mixed with 2 cm³ of pure release medium (diluting) before measuring it in the UV-Vis.

3. Results and Discussion

3.1 Materials Characteristics

The pore textural properties including BET specific surface area are calculated by analysing N_2 adsorption-desorption isotherms at 77 K. The N_2 adsorption plots are provided in Figure 2. The large
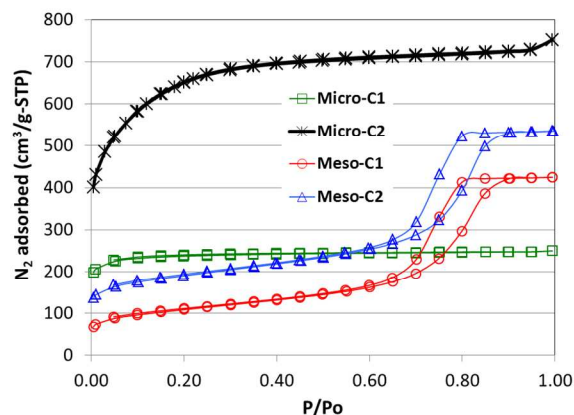
Figure 2. Nitrogen adsorption-desorption plots on Micro-Mesoporous Carbons

Table 1. Pore Textural properties of micro- and mesoporous carbons

Carbon	BET specific surface area (m²/g)	Total Pore volume (cm³/g)
Meso-C1	372	0.63
Meso-C2	641	0.78
Micro-C1	761	0.35
Micro-C2	2251	1.03

hysteresis loop in meso-C1 and meso-C2 confirmed the existence of mesoporosity in those carbons. The isotherms for microporous carbons did not show any hysteresis loop. The BET specific surface area and total pore volume of all the carbons are shown in table 1. It is clear that micro-C2 has the largest BET surface area (2251 m²/g) and total pore volume (1.03 cm³/g). The lowest BET surface area and pore volume is possessed by meso-C1 (372 m²/g and 0.63 cm³/g). Despite high BET surface area and pore volume, microporous carbons did not show significant mesopore distribution.

ARTICLE

RSC Advances

3(a)   3(b)   3(c)

3(d)   3(e)   3(f)

3(g)   3(h)   3(i)

3(j)   3(k)   3(l)
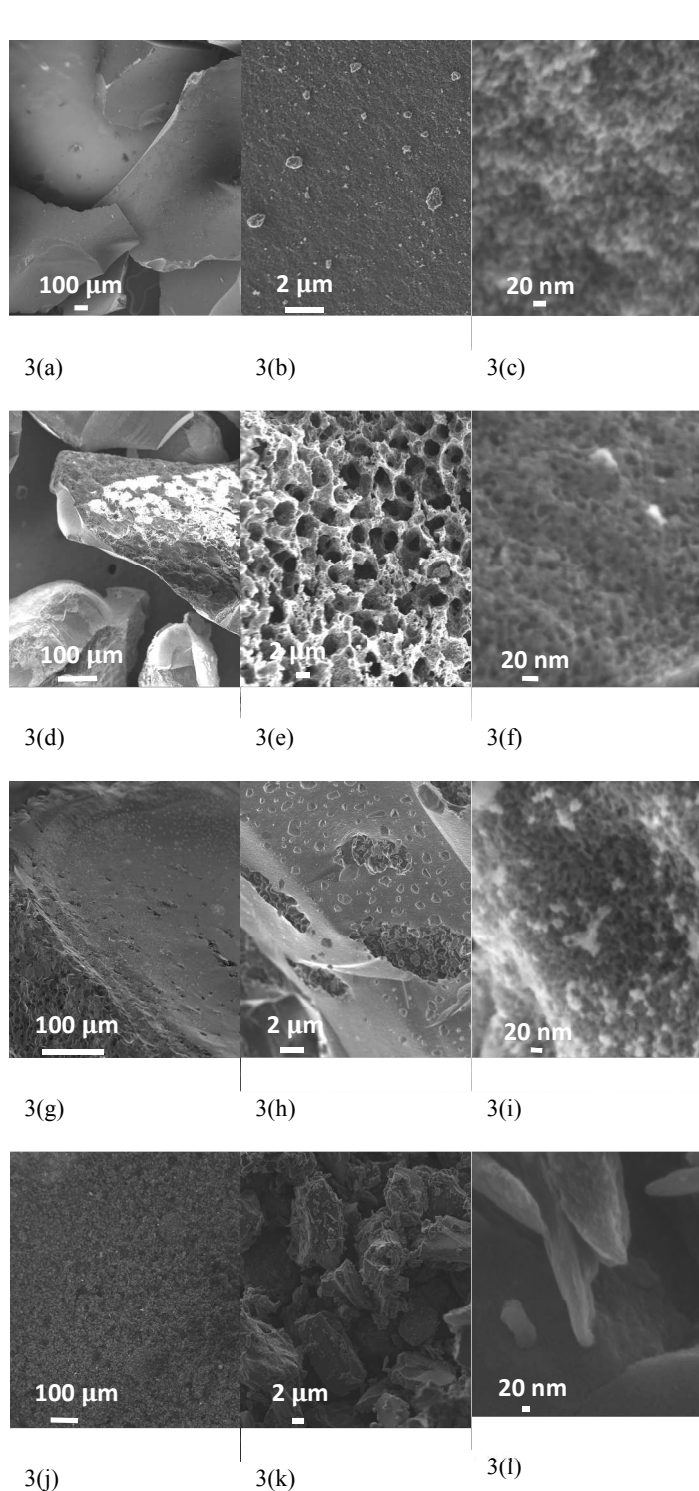
Figure 3. SEM images of the micro-mesoporous carbons; Meso-C1 (a-c), Meso-C2 (d-f), Micro-C1 (g-i), Micro-C2 (j-l).

The scanning and transmission electron microscopic images (SEM and TEM) are provided in Figure 3 and Figure 4. The size of mesoporous carbon samples are larger and in the order of 1400-1500 µm. The size micro-C1 is particles are smaller, about 500 µm, whereas the smallest particles belong to micro-C2, which are in the range of 5-12 µm. The pores that in the order of nanometers are clearly observed for meso-C1, meso-C2 and micro-C1 (Figure 3 (c),

4(a)   4(b)

4(c)   4(d)
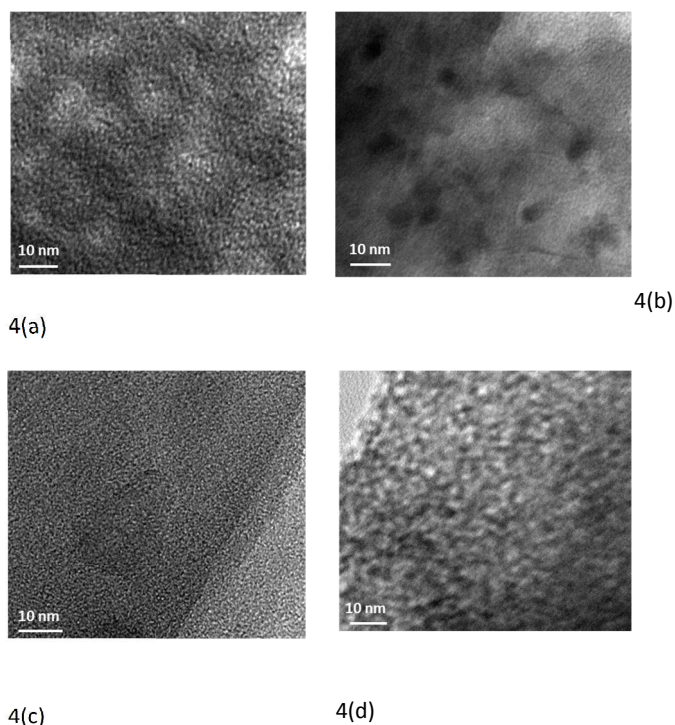
Figure 4. TEM images of Meso-C1(a), Meso-C2(b), Micro-C1(c) and Micro-C2(d)

3 (f) and 3(i)). A network of larger pores, in the order of 4-5 µm are observed for meso-C2 (Figure 3 (e)) that are definitely formed in the course of chemical activation. The array of pores of width less than 1 µm is also observed on the external surface of micro-C1, that can be attributed to the chemical activation. We could not locate the nanozied pores for Micro-C2 by SEM analysis. The TEM image of all the nanoporous carbons reveal that they possess a partial graphitic ribbons and pores are highly disorganized in nature. For micro-C2, the 'worm' shaped pores are clearly visible in the TEM images (Figure 4(d))

3.2 Toxicity studies

The cytotoxicity results in three different carbon concentrations of 50, 300 and 500 µg/mL on *E. Coli* cells are shown in figure 5 and representative light microscopic images on each type of nanoporous carbon samples are shown in Figure 6(a)-6(d). Although we could not locate any trend in bacterial survivor rate with the properties of nanoporous carbons, the results do not correspond to toxic behavior of the carbons. Meso-C1 and Meso-C2 demonstrated slightly lower surviving rate compared to control or blank sample in the lower concentration of 50 and 300 µg/mL and Micro-C2 demonstrated similar trend for 300 µg/mL, but the other concentrations do not corroborate such trends. In the higher concentration, Micro-C1 and Micro-C2 samples depicted even higher surviving rate compared to the blank sample. The higher survivor rate compared to blank sample could be attributed to the fact that bacterial cells preferred the nanoporous carbons as better substrate media to grow and multiply compared to petri-dish; the microscopic images also confirmed that bacteria cells could accumulate surrounding the carbon particles. Positive growth of *E. Coli* bacterial cells compared to control is also observed in literature[23] that reported the survival of bacterial colony in contact with TiO_2 nanoparticles and two polymeric materials, tri-n-octylphosphine oxide (TOPO) and Brij-76. It was attributed to the

possible fact that those materials could promote cellular growth or the bacterial cells might have metabolize them as oligoelement. Such occurrences, if true, may also contribute in our investigations. Although the exact nature of interaction between carbon particles and cells requires much more detailed and controlled study, it can be concluded that the nanoporous carbon samples did not possess significant toxicity to the cells.
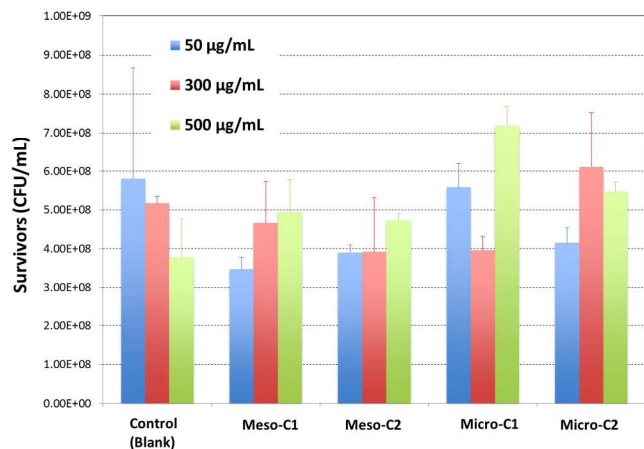
Figure 5. Results of *E. Coli* survival in contact with micro-mesoporous carbons in three different carbon concentrations of 50, 300 and 500 µg/mL
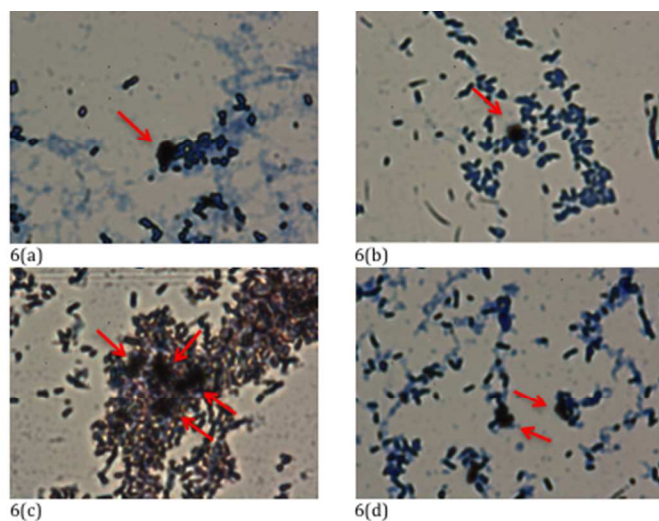
Figure 6. Representative light microscopic images of the *E. Coli* cells in contact with carbon particles; Meso-C1 (a), Meso-C2 (b), Micro-C1 (c), Micro-C2 (d). The carbons particles are marked with arrow(s). All the magnification levels are 1000X

3.3 Mucin adsorption results

Mucin adsorption results for four types of carbons are in the range of 20-30% and showed in Figure 7. The pattern clearly suggests that mucin adsorption increases with the increase in BET surface area (refer to table 1). The other reason of higher mucin adsorption in high surface area carbons may be attributed to the surface affinity. All the three carbons, meso-C2, micro-C1 and micro-C2 were chemically activated with KOH to enhance the surface area. KOH

activation essentially introduces some oxygen functionality on the carbon pore. Such oxygen containing functional groups may form
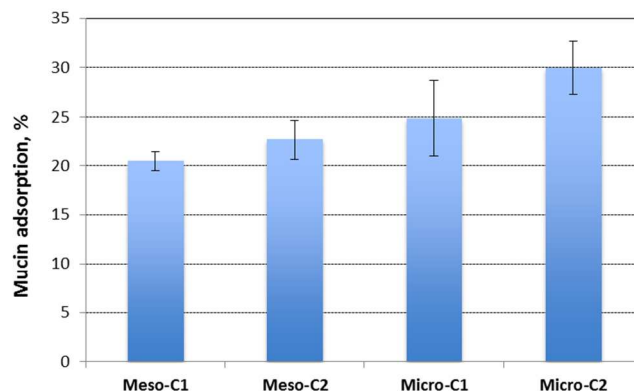
Figure 7. Results of mucin adsorption tests the carbon samples

the hydrogen bonding with the nitrogen atoms of mucin thereby facilitating the overall adsorption. Fair amount of mucin adsorption results suggest that the carbon particles might have a good possibility of adhering to the mucus surface of GI tract and increase its residence time.

3.4 drug loading and release characteristics

Figure 8 represents the loading or adsorption amounts of indomethacin and antipyrine in different nanoporous carbons. The general trend is that the loading amount increases with the increase in surface area. The highest loading is confirmed by micro-C2 for both indomethacin and antipyrine (around 78.8 ± 0.1 %) that has the largest BET SSA, whereas the smallest uptake is manifested by meso-C1 (6.33 ± 0.3 %, for indomethacin; 12.6 ± 0.35 %, for antipyrine) that has the lowest surface area. The minor deviation in
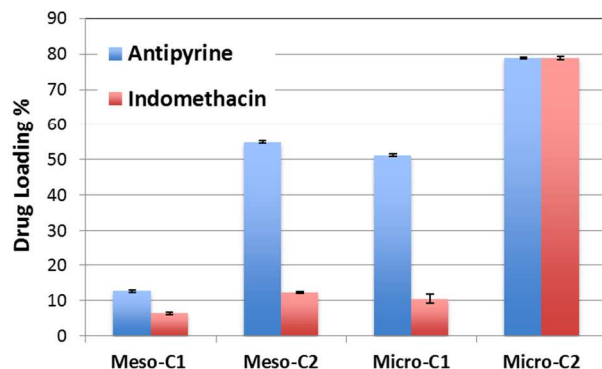
Figure 8. Drug loading amount in carbon samples

such trend occurred for indomethacin and antipyrine adsorption in micro-C1. Although the micro-C1 has slightly higher BET SSA than meso-C2 (761 m^2/g versus 641 m^2/g) it adsorbed slightly lower amount of both drugs compared to the other. Most likely, the higher pore volume of meso-C2 helped to accommodate greater number of molecules of the drug or the presence mesopores in meso-C2 facilitated the transport of the drugs to the micropores. Amount of indomethacin (or antipyrine) uptake by micro-C2 is the largest uptake reported by any porous material, reported so far. In the past study by Karavasili et al[11] for a hard-templated mesoporous carbon,

CMK-3, loading amount of indomethacin was around 15 %, which is similar to that of meso-C2 sample in this study (12.23 ± 0.17 %).

In order to visualize the location of drug loading sites, we have analyzed the differential pore size distribution plot of pure and drug loaded carbons (Figure 9(a)-(e)). Although the outgassing conditions
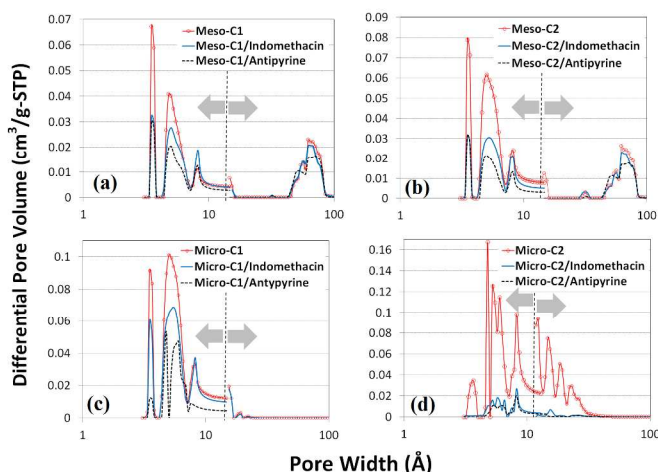
Figure 9. Pore size distribution of pure and drug loaded micro-mesoporous carbon samples; Meso-C1 (a), Meso-C2 (b), Micro-C1 (c), Micro-C2(d). The pore size distribution was calculated by non-local density function theory (NLDFT). The left and right arrow show the data obtained from CO_2 and N_2 adsorption, respectively.

of drug loaded carbons (70-80 °C/24 hours) were not as stringent as pure carbons (300 °C/3 hours) and the drug loaded carbons might also contain few water or ethanol molecules trapped in the narrower pores, such analysis will provide the qualitative view of the pore occupancy by drug molecules. Despite the size of indomethacin is much larger compared to antipyrine (as reported in Fig 1(a) and (b)), indomethacin did not occupy any of the mesopores in meso-C1 and meso-C2, unlike antipyrine that occupied both types of pores. Such anomalous behavior may be attributed to the localized interactions of indomethacin with carbon pore wall, influence of functional groups on the pore and possible orientation and bending of the molecule in the narrower pore space. For micro-C1 and micro-C2, we found that all the pores are partially filled by drug molecules. The largest pore filling of micro-C2 by both indomethacin and antipyrine is clearly correlated with its highest loading capacity (~78%). Unlike rest of carbon samples, micro-C2 possessed the continuous pore widths from 4 to 40 Å. We believe that such hierarchical pore distribution strongly influence that well-facilitated transport of the drug molecules and ultimately help it be adsorbed into the pores.

The comparisons of thermograms of drug loaded carbons with pure drug (Figure 10(a) and 10(b)) clearly showed the presence of drug within the porous carbon moieties. The decomposition peak of pure antipyrine appears around 303 °C, but the peak temperature is shifted around 30 °C more towards the higher temperature side for all antipyrine loaded carbons that may be attributed to the confinement effect in the nanosized pores. For pure indomethacin, the largest peak appears at 328 °C with a very small peak at around 370 °C. In indomethacin loaded carbons, both the peaks became prominent and the shift of peak temperature was much larger compared to antipyrine.

(a)

(b)
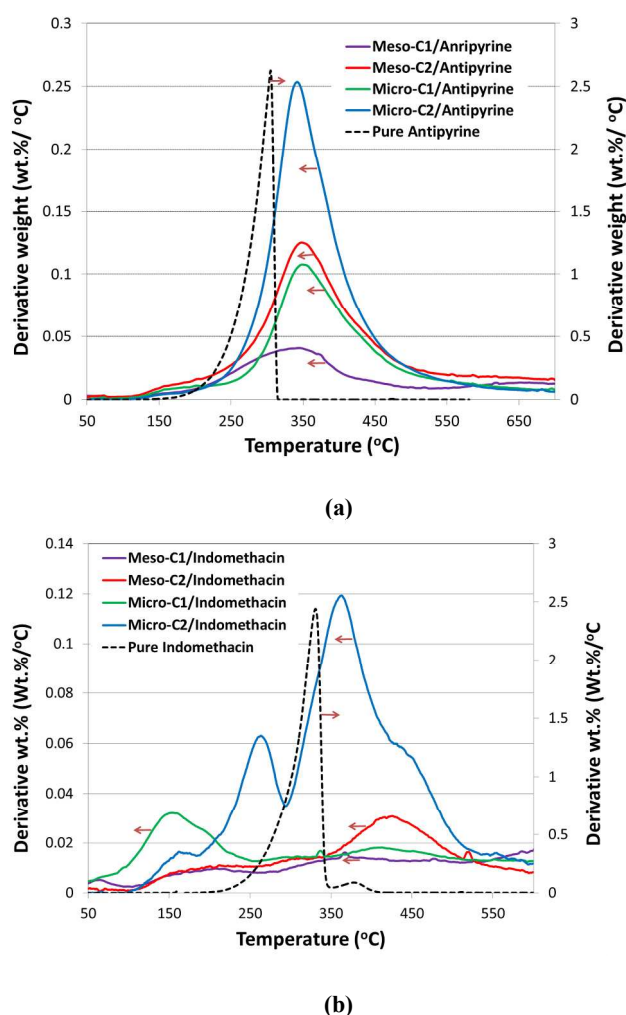
Figure 10. Thermograms of pure drug and drug-loaded carbons for antipyrine (a) and indomethacin (b). The arrows the show the direction of the corresponding Y-axis, Derivative Wt.% (Wt.%/°C).

Intuitively, the confinement-effect as a function of carbon pore size and geometry of drug molecule in accordance with the surface functionality of carbon pores plays the key role in decomposition temperature profile. Further insights onto the precise role carbon pores in confining a particular drug molecules requires much more elaborate study that is beyond the scope of this work.

The release profile of indomethacin in SGF (pH=1.2) and at 37 °C is shown in Fig 11(a). The release rate of drugs from all the nanoporous carbons is faster than pure indomethacin formulation, clearly depicting the beneficial role of nanoporous carbons. Such faster release of Indomethacin is similar with that of submicron sized mesoporous carbon particle synthesized by hard-templating method[24]. Although in our experiment, we found that the release rate reached the saturation level in the time interval of 1 to 3 hours, distinctive saturation time of indomethacin release was reported for different types of formulations. Saturation time was as low as 10 minutes for two types of hard-templated mesoporous carbons[11,24]. The time to reach the saturation level was over 8 hours for chitosan coated hydrogen formulation[25] and 15-20 hours for cross-linked chondroitin in rat cecal material[26] or amino functionalized and carbopol coated MCM-41 in SGF[27].
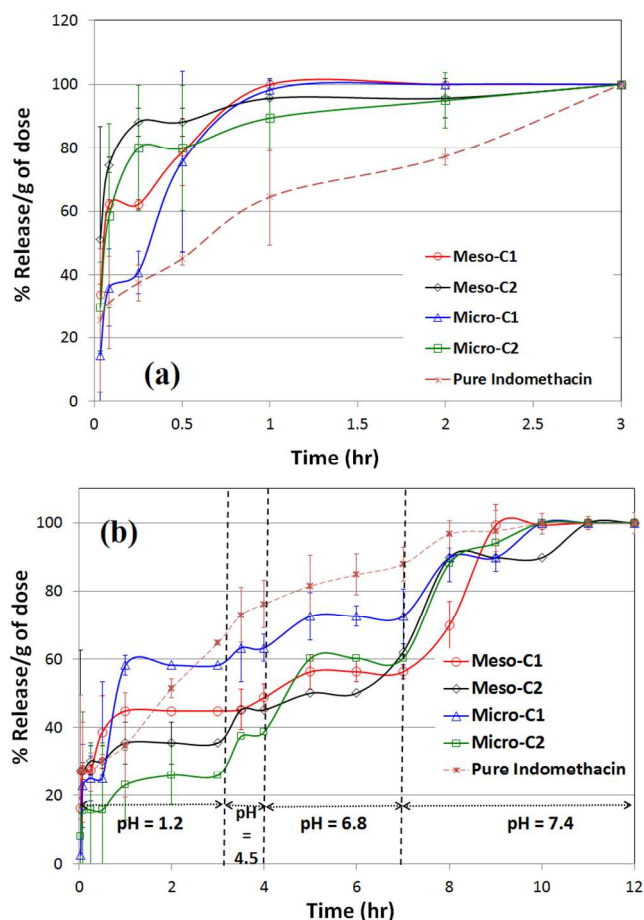
Figure 11. Indomethacin release profile in simulated gastric fluid (SGF) (a) and a combined release profile representing the complete gastro-intestinal (GI) tract (b) All the release experiments were performed at 37 °C.

In order to simulate the release profile of indomethacin loaded nanoporous carbons in the rest of GI tract, we have extended the release experiments in following pH of 4.5, 6.8 and 7.4 at 37 °C and in total 12 hour along with the comparison with pure indomethacin (Fig 11(b)). Such a complete comparison of drug release profile in a varying pH to simulate the entire condition of gastro-intestinal (GI) tract is very rare in the literature[20] and, most likely, does not exist for indomethacin and antipyrine. We found that all the nanoporous carbons that apparently reached the saturation level, continued to release indomethacin for 10-11 hours up to pH=7.4. Most likely, the drug molecules that were adsorbed far inside the pores or narrower pores and within the highest adsorptive force and released in the late period. We found that release from pure indomethacin also leveled off within 10-12 hour period. Indomethacin release from amino functionalized and carbopol coated MCM-41 was 5-8 hours[27] in pH 6.8. The same release rate was 3-10 hours in pH 6.5, 6.8 and 7.2 for methacrylate loaded formulation[28] or 10-15 hours for thermo-responsive polyvinyl alcohol or polyacrylic acid[29] in pH 7. In few instances, the release rate was extremely slow and in the order of days. The release of indomethacin was 20-30 hours from diatom silica[30] in pH 7.4 and over 10 days from nanocomposites of silica gel[31]. It also took over 15-20 days to reach the saturation level for PEG coated zirconia particle in simulated body fluid (SBF)[32]. The high release time for porous media may be attributed to the

accumulation of drug in crystalline form on outside or in macropores that took elongate time to gradually dissolve or leach out in the release media for the extended interval of time. For the polymeric formulations, the cause may be far more complicated, it can be related to polymer-drug interactions or entrapment of drug by polymer layer. It can be clearly stated that, for oral delivery of a poor soluble drug like indomethacin, the release rate should be designed as fast as possible in order to benefit the high rate of dissolution and absorption in the GI tract.

Release experiment of antipyrine in simulated gastric fluid (SGF) at 37°C (Figure 12(a)) reveals that all the nanoporous carbons release almost 90% of saturation level within an hour and gradually reached the saturation level in over two hour period.
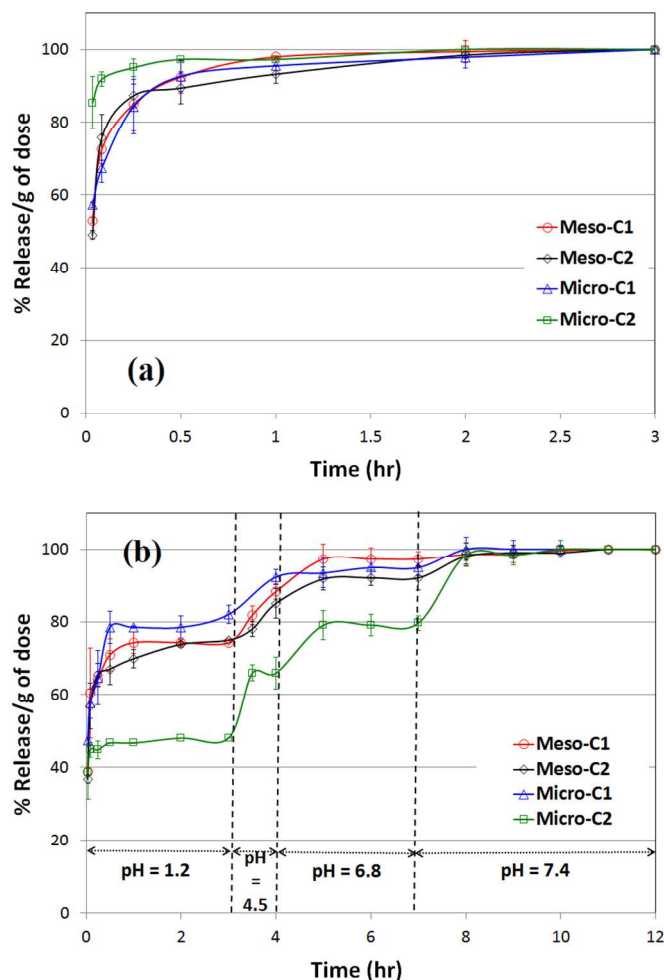
Figure 12. Antipyrine release profile in simulated gastric fluid (SGF) (a) and a combined release profile representing the complete gastro-intestinal (GI) tract (b). The release profile of pure antipyrine was not shown because of its instant solubility in aqueous solutions. All the release experiments were performed at 37 °C

Amongst all the carbons, micro-C2 showed the fastest release; over 80% of saturation level occurred in the first burst release. Most likely, the drug molecules that were present in the outer periphery of pores, released in this time. Such release profile is very similar to that of released from phloroglucinol derived mesoporous carbons at

35.5 °C, but quite faster than that from lignin derived mesoporous carbons[18].

The complete release profile of antipyrine in all the four pH values at 37°C is shown in Figure 12(b). Unlike release pattern in SGF, micro-C2 sample maintained the sustained release for the longest interval of time, upto 8-9 hours. There is no significant difference in the release patterns amongst rest of the carbon samples, they reached the 90-95% of saturation level in five hour period. The reason of best-sustained release pattern of micro-C2 can most likely be attributed to the largest drug uptake and variable pore width, as observed in Figure 9d. Most likely, it started to dissolve from largest pore and eventually reached the narrower pores at the end of the release pattern. Additionally, the narrower pores exerted the strongest adsorptive force on the drug molecules resulting its release mostly delayed. Such release profile is more delayed than that from porous silica in pH 7.4 reported by Salonen et al. [33]. Release of antipyrine was as high as 6 hours from organogels in simulated intestinal fluid[34]. It is also reported that release of antipyrine was delayed as much as 6 to 11 hours in different release media by employing the swollen gels of hydroxypropyl methyl cellulose of (HPMC)[35] or other microcrystalline cellulose compositions[36]. Such evidence suggests that compositing of nanoporous carbons with polymeric materials may improve its performance for the sustained release of hydrophilic drugs.

4. Conclusions

In this phase of research, we have employed four types of micro- and mesoporous carbons for the controlled release purposes of two model drugs, indomethacin (aqueous insoluble) and antipyrine (aqueous soluble). The micro-mesoporous carbons were characterized with BET surface area and pore volume that are in the range of 372-2251 m^2/g and 0.63-1.03 cm^3/g, respectively. Neither of the carbon samples demonstrated significant toxicity in the bacteria culture studies. The drug loading amounts were 6-78%, where the highest amount of drug loading was manifested by micro-C1 that possesses the highest BET surface area and pore volume. The drug release experiments were performed in SGF and in three other different media with varying pH and residence time to mimic the physiological conditions of actual gastrointestinal (GI) tract. Both the carbons demonstrated sustained release profile that confirmed that these materials can be employed as potential drug carriers.

References

1 U. Edlund, A.C. Albertson, *Advances in Polymer Sci.,* 2002, **157**, 67.

2 M. Arruebo, *Wiley Interdisciplinary Rev: Nanomed. Nanobiotechnol.* 2012, **4**, 16.

3 B.N. Singh, K.H. Kim, *J. Controlled Release* 2000, **63**, 235.

4 M. Vallet-Regi, F. Ballas, D. Arcos, *Angew. Chem. Intl. Ed.* 2007, **46**, 7548.

5 P. Yang, S. Gai, J. Lin, *Chem. Soc. Rev.* 2012, **41**, 3679.

6 W. Xu, J. Riikonen, V.-P. Lehto, *Intl. J. Pharmaceutics* 2013, **453**, 181.

7 I.I. Slowing, J.L. Vivero-Escoto, C.-W. Wu, V.S.-Y. Lin, *Adv. Drug Delivery Rev*. 2008, **60**, 1278.

8 C.Barbe, J. Bartlett, L. Kong, K. Finnie, H. Q. Lin, M. Larkin, S. Calleja, A. Bush, G. Calleja, *Adv. Mater.* 2004, **16**, 1959.

9 I. I.Slowing, B. G.Trewyn, S. Giri, V. S.-Y. Lin, *Adv. Funct. Mater.* 2007, **17**, 1225.

10 X.Wang, P. Liu, Y. Tian, L. Zang, *Microporous Mesoporous Mater.* 2011, **145**, 98.

11 C. Karavasili, E. P.Amanatiadou, L.Sygellou, D. K. Giasafaki, T. A. Steriotis, G. C. Charalambopoulou, I. S. Vizirianakis, D. G. Fatouros, *J. Mater. Chem. B* 2013, **1**, 3167.

12 P. Zhao, L. Wang, C. Sun, T. Jiang, J. Zhang, Q. Zhang, J. Sun, Y. Deng, S.Wang, *Eur. J. Pharm. Biopharm.* 2012, **80**, 535.

13 J. Zhu, L. Liao, X. Bian, J. Kong, P. Yang, B. Liu, *Small* 2012, **8,** 2715.

14 J. Gu, S. Su, Y. Li, Q. He, J. Shi, *Chem. Commun.* 2011, **47**, 2101.

15 A. Labiano, M. Dai, D. Taylor, W.-S. Young, T. H. Epps III, K. Rege, B. D. Vogt, *Microporous Mesoporous Mater*. 2012, **160**, 143/ doi:10.1016/j.micromeso.2012.05.003.

16 D. Saha, E. A. Payzant, A. S. Kumbhar, A. K. Naskar, *ACS Appl. Mater. Interfaces* 2013, **5**, 5868.

[17] D. Saha, K. E. Warren, A. K. Naskar, *Carbon* 2014, **71**, 47/ doi:10.1016/j.carbon.2014.01.005.

[18] D. Saha, K. E. Warren, A. K. Naskar, *Microporous Mesoporous Mater.* 2014, **196**, 327./ doi:10.1016/j.micromeso.2014.05.024.

[19] M.F. Gencoglu, A. Spurri, M. Franko, J. Chen, D.K. Hensley, C.L. Heldt, D. Saha, *ACS Appl. Mater. Interfaces,* 2014, **6**, 15068.

[20] L. Sun, Y. Wang, T. Jiang, X. Zheng, Zhang, J. Sun, C. Sun, S. Wang, *ACS Appl Mater Interfaces* 2013, **5**, 103.

[21] J. Filipovic-Grcic, N. Skalko-Basnet, I. Jalsenjak, *J. Microencapsul.* 2001, **18**, 3.

[22] H.K. Han, H.-J. Shin, D.H. Ha, *Eur. J. Pharm. Sci.* 2012, **46**, 500.

[23] R. Brayner, R. Ferrari-iliou, N. Brivois, S. Djediat, M.F. Benedetti, F. Fievet, *Nano. Lett.* 2006, **6**, 866.

[24] S.C. Shen, W.K. Ng, L.Z.O. Chia Y.-C. Dong, R.B.H. Tan, *Powder Technol.* 2014, **261**, 241.

[25] O. Munjeri, J.H. Collett, J.T. Fell. *J. Controlled Release* 1997, **46**, 273.

[26] A. Rubinstein, D. Nakar, A. Sinto, *Pharmaceutical Research* 1992, **9**, 276.

[27] B. Tzankov, K. Yoncheva, M. Popova, A. Szegedi, G. Momekov, J. Mihály, N. Lambov, *Microporous and Mesoporous Mater.* 2013, **171**, 131/ doi:10.1016/j.micromeso.2012.12.037.

[28] A. Akhgari, H.A. Garekani, F. Sadeghi, M. Azimaie, *Intl. J. Pharm.* 2005, **305**, 22.

[29] H.S. Shin S.Y. Kim, Y.M. Lee. *J. Appl. Polymer Sci.* 1997, **65**, 685.

[30] M. Barianba, M.S. Aw, D. Losic, *Adv. Powder Technol.* 2013, **24**, 757.

[31] J.H. Chang, C.H. Shim, B.J. Kim, Y. Shin, G.J. Exerhos, K.J. Kim, *Adv. Mater.* 2005, **17**, 634.

[32] . M. Catauro, F. Bollino, F. Papale, S. Pacifico, S. Galasso, C. Ferrara, P. Mustarelli, *Drug Deliv.* 2013, **21**, 595.

[33] J. Salonen, L. Laitinen, A.M. Kaukonen, J. Tuura, M. Bjorkqvist, T. Heikkila, K. Vaha- Heikkila, J. Hirvonen, V.-P. Lehto, *J. Controlled Release* 2005, **108,** 362.

[34] K. Iwanaga, M. Kawai, M. Miyazaki, M. Kakemi, *Intl. J. Pharm.* 2012, **436,** 869.

[35] C. Dahlberg, A. Fureby, Schuleit, S.V. Dvinskikh, I. Furó, *J. Controlled Release* 2007, **122,** 199.

[36] M.E. Sangalli, A. Maroni, L. Zema. F. Giordano, A. Gazzabiga, *J. Controlled Release* 2001, **73**, 103.